NuLIMAS
numerical modelling of liquefaction around marine structures

Leichtweiß-Institut

Technische Universität Braunschweig

Numerical modelling of liquefaction around marine structures

White Paper

June, 2022

Abstract

Liquefaction around marine structures can lead to severe structural failure and the susceptibility of seabed soil to liquefaction at a specific installation site of, e.g., floating offshore wind turbines should be included within the design process and site evaluation. To that end, advanced prediction tools based on numerical modelling can provide valuable insight into the hydro-geotechnical processes. However, developing a holistic modelling of seabed liquefaction is a challenging task, due to the complex interaction of the underlying physics. **The NuLIMAS project (Numerical modelling of liquefaction around marine structures)** aims at the development of a numerical model of seabed liquefaction in the OpenFOAM® framework. This white paper provides an overview of the NuLIMAS project and presents initial results of the model development.

NuLIMAS receives funding through the ERA-NET Cofund MarTERA and is a joint research project of the Leichtweiß-Institute for Hydraulic Engineering and Water Resources, Großmann Ingenieur Consult (GICON) GmbH, WIKKI Gesellschaft für numerische Kontinuumsmechanik mbH, BM SUMER Consultancy & Research, the Institute of Hydro-Engineering of Polish Academy of Sciences, and Projmors Designing Office For Maritime Structures Company Limited.

1 Introduction

Throughout the past decades, an increasing exploitation of the marine environment can be observed. Next to traditional oil and gas exploration or the shipping industry, novel players, such as aquaculture or marine energy, are entering the offshore environment.

Offshore wind can clearly be highlighted as one of the driving technologies amongst the marine renewable energy systems. A transition towards higher abundant wind speeds (and thus wind resource) at deep water depths (i.e. $d > 50\,\mathrm{m}$) can be observed for the offshore wind industry. At such deep water depths, floating offshore wind turbines (FOWT, see Figure 1) become economically feasible, compared to their bottom fixed counterparts.

Among the different engineering challenges, seabed liquefaction around the anchoring structures of FOWTs needs to be considered; however, is often under-explored. **Seabed liquefaction describes the phenomenon by which the seabed soil loses its bearing capacity** and acts like a highly viscous fluid due to the accumulation of pore pressure [1]. It is obvious that such a loss of bearing capacity can lead to severe system failure [2, 3, 4].

The modelling, analysis, and prediction of seabed liquefaction renders challenging, due to the highly complex interaction of the hydrodynamic and geotechnical processes.

Figure 1: Artist's impression of GICON®'s tension leg platform (TLP)-type FOWT concept (courtesy of GICON®)

The NuLIMAS project aims to address shortcomings of current numerical modelling approaches by developing a novel, OpenFOAM® –based, numerical model. This white paper provides an overview of the NuLIMAS projects and presents initial results of the model development. The model development can be separated into the three steps:

(i) Numerical implementation;

(ii) Model calibration;

(iii) Model validation.

For steps (ii) and (iii) dedicated experimental test campaigns are planned within the NuLIMAS project. In particular, for the model validation, the **GICON® TLP–type FOWT is employed as case study**.

2 Seabed liquefaction

Seabed soil can lose its bearing capacity due to the accumulation of pore pressure. This accumulation of pore pressure and, thus, seabed liquefaction, is triggered by cyclic shear stress induced, for instance, by seismic loading or cyclic surface wave action. Within NuLIMAS, only wave-induced liquefaction is considered.

The physical processes leading to seabed liquefaction are schematically depicted in Figure 2: When applying shear stress on a volume of loosely packed soil, the soil grains may rearrange, thus showing a tendency to contract, resulting in a decrease of pore volume within the soil. The decrease of the pore volume leads to an increase in pore pressure and, in turn, a tendency of the pore water to flow out of the pore volume. If the soil volume is able to drain, the increased pore pressure dissipates (Figure 2 (b.1)). In undrained conditions, the pore pressure does not dissipate and, if shearing continues, accumulates (Figure 2 (b.2)). Following Terzaghi's principle, the increased pore pressure results in a reduction of the normal effective stress in the soil volume up to a point where the soil effectively looses it's bearing capacity (Figure 2 (c)). A detailed description of seabed liquefaction can be found in [5, 6].

After liquefaction is triggered, a pore pressure gradient leads to a settling of soil grains. This compaction

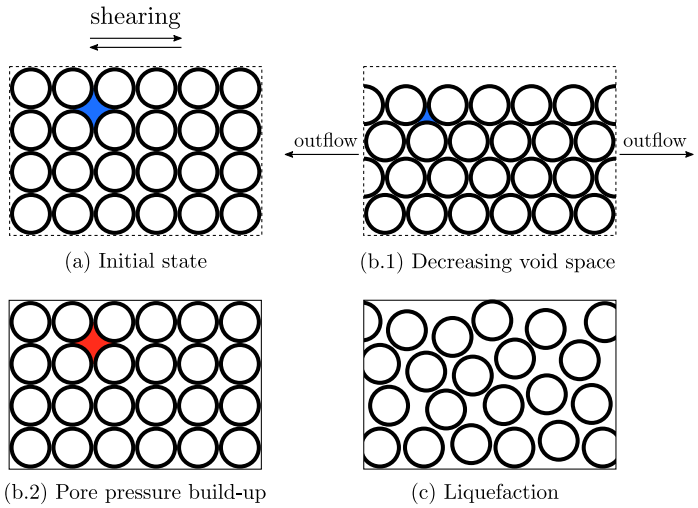

(a) Initial state (b.1) Decreasing void space

(b.2) Pore pressure build-up (c) Liquefaction

Figure 2: Schematic representation of the physical processes leading to seabed liquefaction. The blue void indicates low pore pressure, the red void indicates high pore pressure.

(i.e. change of state from liquid to solid) starts from the impermeable base, moving towards the mud line.

2.1 Modelling of seabed liquefaction

Considering the seabed soil as poro-elastic solid soil, models to describe the governing quantities, i.e. the pore pressure and shear stresses, are described by Biot's theory on poro-elasticity [7].

Two equations are derived for the linear momentum balance and the pore fluid continuity. The total momentum balance of the poro-elastic solid is achieved when the equilibrium conditions of the stress field are satisfied, i.e.

$$\nabla \cdot \sigma = 0\,. \tag{1}$$

In a poro-elastic soil, the normal stress can be decomposed in the effective stress, σ', carried by the soil skeleton, and the pore fluid pressure, p.

Following this decomposition and applying Hooke's law, the equilibrium of poro-elastic soil reads,

$$G\nabla^2 U + \frac{G}{1-2\nu}\nabla\epsilon = \nabla p\,, \tag{2}$$

where G denotes the shear Modulus, ν is the Poisson ratio,

and U denotes the displacement vector. ϵ denotes the volume increase per unit volume of soil.

Applying Darcy's law, the continuity equation for the pore water is formally expressed by

$$\frac{k}{\gamma}\nabla^2 p = \frac{n}{K'}\frac{\partial p}{\partial t} + \frac{\partial \epsilon}{\partial t}\,, \tag{3}$$

where k denotes the hydraulic conductivity and γ denotes the specific weight of the soil. K' is the true bulk modulus of elasticity of water. **Equations (2) and (3) are commonly referred to as the Biot consolidation equations.** Depending on the inclusion of inertial effects, three formulations are available:

(i) Quasi-steady: Both the acceleration of the soil skeleton and the acceleration of the pore water relative to the soil skeleton are ignored (original Biot equations, as shown in (2) and (3))

(ii) Partially dynamic: Only the acceleration of the soil skeleton is considered

(ii) Fully dynamic: Both the acceleration of the soil skeleton and the acceleration of the pore water relative to the soil skeleton are considered

2.1.1 Pore pressure buildup

The Biot consolidation equations (2) and (3) do not include solutions for the pore pressure to build up under progressive waves. Sumer [6] delivers a **description for the pore pressure buildup**, following

$$\frac{\partial P}{\partial t} = c_v \frac{\partial^2 P}{\partial z^2} + f\,, \tag{4}$$

where P is the accumulated pore pressure, c_v is the coefficient of consolidation, and f denotes a source term. The source term f represents "the total amount of averaged pore pressure generated per unit time per unit volume of soil" [6, p. 75] and follows

$$f = \frac{\sigma_0'}{N_\ell T}\,, \tag{5}$$

where N_l denotes the number of cycles required until onset of liquefaction, σ_0' denotes the initial mean normal effective stress, and T is the wave period. An expression for N_l, as a function of the shear stress amplitude, A_τ, can be found in [8].

2.1.2 Liquefaction criterium

Residual liquefaction (see Figure 2 (c)) sets in when the accumulated pore pressure is larger than the initial mean normal effective stress:

$$\frac{P}{\sigma_0'} > 1\,. \tag{6}$$

A validation of the above described model for the pore-water pressure buildup under progressive waves is presented in [9]. For a more detailed derivation of the model, the interested reader is referred to [6].

3 State-of-the-art

A large number of analytical, numerical, experimental, and field studies concerning various aspects of seabed liquefaction can be found in the literature. Reviews of these studies are, for instance, presented in [10, 11, 12].

Based on Biot's poro-elasticity theory, numerous numerical models have been developed to analyse seabed dynamics. Such models, generally, deliver higher accuracy compared to analytical models; however, require more computational effort. In his review, Jeng [10] differentiates between numerical models based on finite differences, finite elements, and the boundary element method. Early models have been developed in, e.g., [13, 14, 15]

While the early numerical models focus more on the process level of seabed dynamics and liquefaction, more recently, engineering problems, by means of wave–structure–soil interaction (WSSI), are considered.

Jeng *et al.* [16] propose an integrated model for WSSI based on the Volume-Averaged Reynolds-Averaged Navier–Stokes (VARANS) equations to incorporate wave modelling and the dynamic Biot equations for the porous elastic seabed. Discretisation is achieved via the finite element method. The model is employed for the analysis of the dynamic response of a large-scale composite breakwater.

Also employing an integrated model with the Reynolds-Averaged Navier-Stokes (RANS) equations for the mean fluid flow and the Biot equations for the seabed, Zhao *et al.* [17] analyse the seabed response around a monopile foundation. Finite differences and finite elements are used to discretise the hydrodynamic and geotechnical problem, respectively.

Recently, also the finite–volume method is used to discretise WSSI problems. **Elsafti and Oumeraci [18] and Li *et al.* [19] propose modelling frameworks, implemented in the open source CFD toolbox OpenFOAM®.** Both of the numerical models can be applied to predict the onset of momentary liquefaction.

To validate the developed numerical models, experimental data are commonly considered as reference. Experimental studies can generally be divided based on the test facility, i.e. centrifuges or wave tanks/flumes [11]. While test campaigns in centrifuges overcome issues related to the stresses due to the soil self-weight, these test facilities are rather complex and wave generation within centrifuges is challenging. When comparing the non-dimensional pore pressure, Sumer [6] shows that results from wave flume tests can deliver satisfying agreement with centrifuge tests.

Similar to the numerical modelling, experimental test campaigns are conducted to analyse seabed liquefaction on the process level (e.g. [5, 9]), but also to address engineering problems related to WSSI.

Sumer *et al.* [20] conduct experiments on the dynamic behaviour of a pipeline in liquefied soil under waves, performing parameter studies to investigate the effect of, e.g., the specific gravity or the soil layer thickness, on the behaviour of the pipeline. A related study on the sinking of irregular blocks in liquefied soil can be found in [21].

Kudella *et al.* [22] perform large scale experiments on the soil response underneath a caisson breakwater due to wave action. The authors find that the rocking motion of the breakwater is the main driver for the accumulation of pore pressure. Based on this finding, Sumer *et al.* [23] conduct experiments with a vibrating plate, performing parameter studies on the effect of amplitude and period of the plate motion on the pore pressure.

From the numerical studies in the literature, it can be observed that no holistic numerical model for seabed liquefaction, including pore pressure buildup, liquefaction, and compaction, is available. Reviewing the experimental studies, it can be concluded that none of the studies are dedicated for the calibration and validation of numerical models. Hence, the studies usually lack some crucial information, hampering thorough model validation. **These shortcomings motivate the NuLIMAS project to develop a holistic, OpenFOAM® –based, numerical model for seabed liquefaction, accompanied by dedicated experimental studies for model calibration and validation.** The model aims to represent residual liquefaction, which also includes soil modelling after liquefaction until compaction.

4 Numerical approach

On the basis of an idealised representation of an offshore floating platform (see Figure 1), such a model needs to include three different regions (see Figure 3): the waves above the seabed (Ω_1), the solid soil region (Ω_2), and, finally, the liquefied region (Ω_3). In addition, the gravity anchor is represented as an idealised rigid body with six degrees of freedom with mooring forces acting upon it.

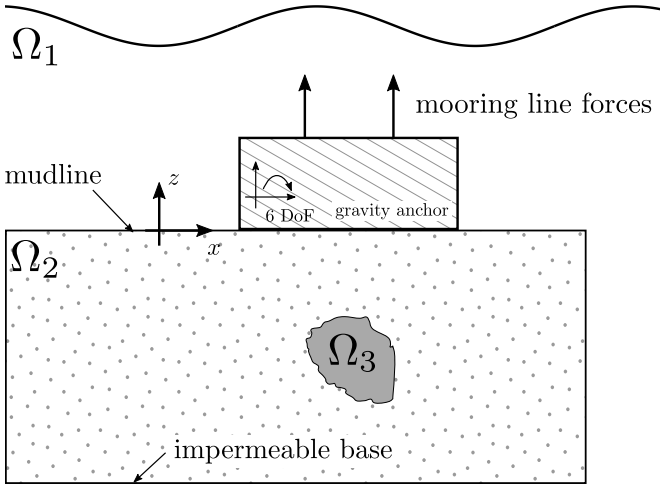

Figure 3: Schematic of the numerical setup. (Figure adapted from [24].)

4.1 Initial model

In a first step towards a holistic model of seabed liquefaction, the `biotFoam` solver within OpenFOAM® [25] has been extended to incorporate pore pressure buildup [24]. In the new `pressureBuildupFoam` solver, the equation (4) is solved to calculate the pore pressure buildup. The source term in Equation (4) depends on the initial mean normal effective stress, the number of cycles for liquefaction (amplitude of shear stress), and the time period. In `pressureBuildupFoam`, the amplitude of the shear stress A_τ is calculated from the root mean square of the shear stress, τ_{rms}.

The calculation via the root mean square is not accurate until the end of the first wave period. To overcome this issue, `biotFoam` is initially used to calculate the shear stress. The preliminary simulation is performed for a sufficiently long simulation time to ensure an accurate calculation of the steady state amplitude of the shear stress. This steady-state amplitude of the shear stress is then used in the initial iteration of `pressureBuildupFoam`.

With the results for the source term f, the equation for the pore pressure build (Equation (4)) is solved and a check for the liquefaction can be performed (Equation (6)). The flow chart of solution procedure in `pressureBuildupFoam` is shown in Figure 4.

4.1.1 Boundary conditions

In this initial model, the effect of progressives waves on the seabed is implemented via of a pressure boundary condition at the mudline, where the harmonic oscillation of the pressure is expressed by a sine function with an amplitude and a phase. In addition to the pressure boundary condition, a traction free displacement boundary is implemented at the mudline.

For a displacement boundary condition, the gradient boundary can be derived from the traction force by representing stress in terms of displacement [26]. For more details on the implementation, including the source code, see [24].

4.1.2 Results

By way of example, initial results of a simple test case for the use of `pressureBuildupFoam` are shown in the following. The numerical domain, including the boundary conditions, is depicted in Figure 5. Waves are acting on the soil domain, represented by a pressure of amplitude p_0 and with an angular frequency ω. All relevant parameters (wave height, soil depth, etc.) are adapted from [6, 27] and are listed in Table 1.

Table 1: Physical properties of the wave and seabed

Physical property	Value	Unit
Water depth d	19	m
Wave height H	6	m
Wave frequency ω	0.46	$\mathrm{rad\,s^{-1}}$
Soil depth h	1	m

The results of the nondimensionalised accumulated pore pressure P/σ_0' along the soil column for different time instances are shown in Figure 6. The results indicate that the pore pressure along the soil column is building up over time. After 15 minutes, the top of the seabed ($z/h > -0.6$) fulfils the liquefaction criterion. For a more detailed discussion of the results and additional test cases, the interested reader is referred to [24].

5 Experimental approach

Validation of the NuLIMAS toolbox against experimental results is desired. In particular for the extension of the current numerical model to include the liquefied soil. To validate the numerical model, sufficient calibration of the user defined soil parameters may be required. Consequently, two experimental test campaigns will be conducted in the course of the NuLIMAS project. At small scale, experiments on the process level are planned, primarily focused on the model calibration. At larger scale, a test campaign on the system level, using GICON®'s TLP–type FOWT, is planned, primarily focused on model validation.

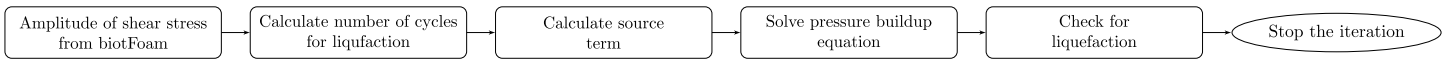

Figure 4: An outline of the solution procedure for a single iteration in `pressureBuildupFoam`. (Figure adapted from [24].)

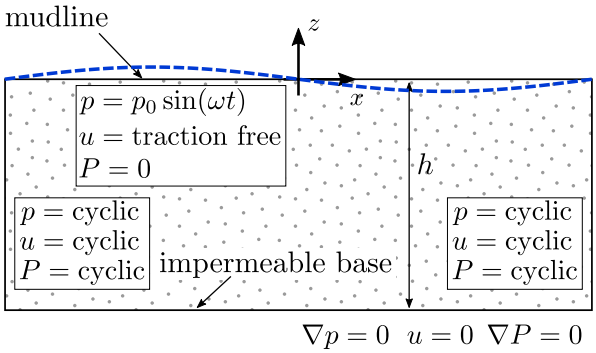

Figure 5: Schematic of the numerical setup for the onset of liquefaction. Figure adapted from [24].

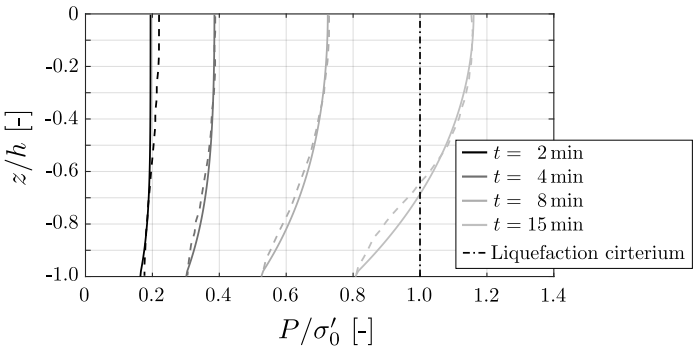

Figure 6: Comparison of the numerical (solid) and analytical [6] (dashed) non-dimensional pore pressure along the soil column at different time instances. Figure adapted from [24].

5.1 Small scale

Four different tests are planned at small scale. First, wave–soil interaction is analysed (see Figure 7 (a)). A sand section is prepared in the **wave flume at the Institute of Hydro-Engineering of the Polish Academy of Sciences** and waves of varying height ($0.05\,\mathrm{m} \leq H \leq 0.20\,\mathrm{m}$) and period ($0.9\,\mathrm{s} \leq T \leq 1.7\,\mathrm{s}$) are induced in the flume, while the pore pressure is monitored at various locations within the sand section. The flume has an overall length of $64\,\mathrm{m}$, a width of $0.6\,\mathrm{m}$ and enables water depths of up to $0.8\,\mathrm{m}$. For the experiments, a sand section with a length of $1\,\mathrm{m}$ is included in the flume and the water depth is set to $0.5\,\mathrm{m}$.

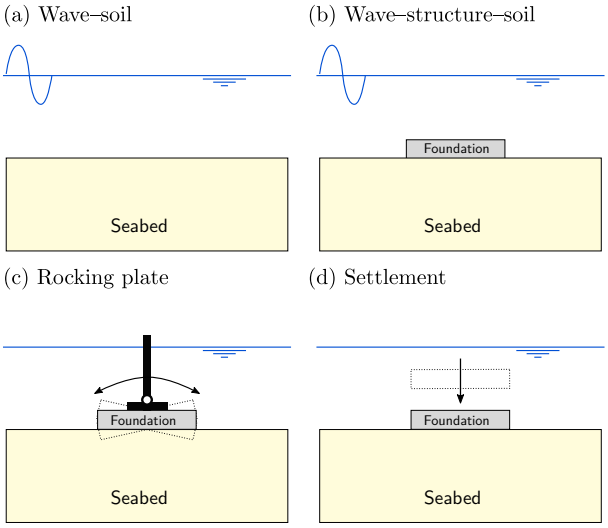

Figure 7: Schematic depiction of the small scale experimental test setup.

To introduce WSSI, a small scale gravity anchor, resembling the gravity anchor of GICON®'s FOWT system, is placed on the sand section in the flow (see Figure 7 (b)). Again, waves of varying height and period are induced in the flume, while the pore pressure is monitored at various locations within the sand section. The motion of the foundation is monitored via video capturing through the glass walls of the flume.

In a next step, the experiments by Sumer *et al.* [23] are adapted (see Figure 7 (c)). The scaled gravity anchor is excited to perform oscillatory rocking motion. No waves are progressing through the flume. As for the previous tests, the pore pressure is monitored at various locations within the sand section.

Finally, the pore pressure in the sand section during the settlement/installation process of the gravity anchor is studied. No waves are progressing through the flume

and the gravity anchor is lowered onto the sand section.

For all small scale experiments, a scaling factor of $1/75$ is chosen. The soil is chosen based on the soil characteristics in [9] and a characterisation of the soil has been performed prior to the start of the flume experiments.

5.1.1 Initial results

In the following some results of the wave–soil test cases are presented. Figure 8 shows photographs of the wave–soil interaction post–liquefaction in the wave flume for waves with a wave height $H = 0.1\,\mathrm{m}$ and a wave period of $T = 1.3\,\mathrm{s}$. The photographs clearly indicate the liquid–like behaviour of soil and its reaction to the surpassing waves. A clear phase shift between the deflection of the mudline and the free surface elevation can be observed at $t = 0.50\,T$ and $t = 1.00\,T$.

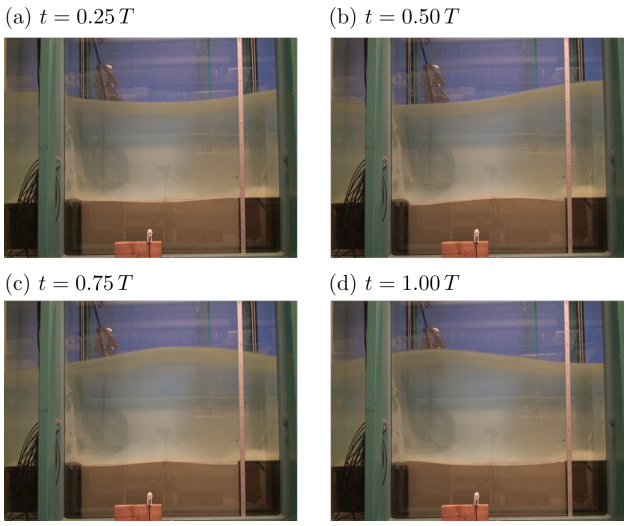

Figure 8: Photographs of the wave–soil interaction in the wave flume for waves with a wave height $H = 0.1\,\mathrm{m}$ and a wave period of $t = 1.3\,\mathrm{s}$.

A more quantitative analysis is delivered in Figure 9, showing the pore pressure evolution over time at various depths of the soil column, i.e. (a) $z = 0.10\,\mathrm{m}$; (b) $z = 0.15\,\mathrm{m}$; (c) $z = 0.20\,\mathrm{m}$; (d) $z = 0.25\,\mathrm{m}$. The plots include results for four different wave heights $(0.05,\ 0.10,\ 0.15,\ 0.20\,\mathrm{m})$. The initial mean normal effective stress σ'_0 is represented by the dashed black line.

It can clearly be seen that the smallest wave height $(H = 0.05\,\mathrm{m})$ does not trigger liquefaction, i.e. $P < \sigma'_0$, throughout the course of the experiment. To the contrary, the higher wave heights do surpass the liquefaction criterion shortly after the start of the experiment. In particular, the two highest wave heights $(0.15,\ 0.20\,\mathrm{m})$ result in $P > \sigma'_0$ after less then $0.2\,\mathrm{min}$.

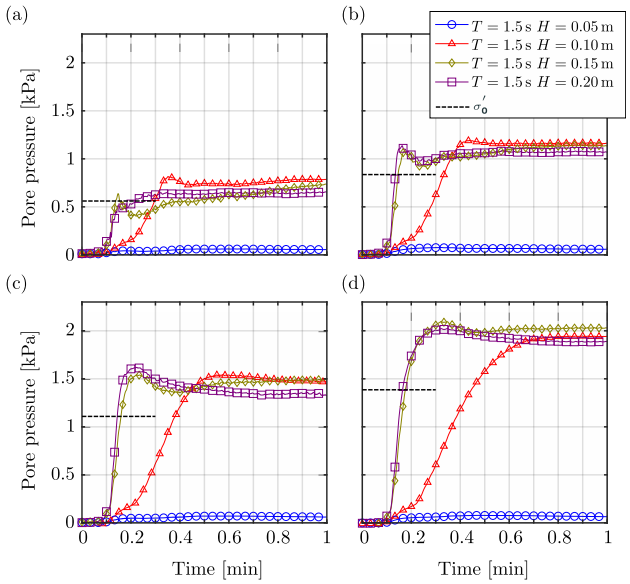

Figure 9: Time traces of the pore pressure measured at for different vertical positions in the sand section. (a) $z = 0.10\,\mathrm{m}$; (b) $z = 0.15\,\mathrm{m}$; (c) $z = 0.20\,\mathrm{m}$; (d) $z = 0.25\,\mathrm{m}$. The horizontal position of the transducers is fixed at the centre of the sand section.

5.2 Large scale

While the small scale experiments focus on the process level of seabed liquefaction and provide calibration data for the numerical model, the large scale experiments focus on a system level, aiming at providing data for numerical model validation. The large scale experiments resemble GICON®'s TLP–type FOWT. A schematic of the experimental setup for the large scale experiments is shown in Figure 10. A scale of approx. $1/15$ is targeted.

The experiments will be conducted in the **large wave flume GWK+ at the coastal research centre, Hannover, Germany**. The wave flume has a length of $300\,\mathrm{m}$, a width of $5\,\mathrm{m}$, and a water depth of $5\,\mathrm{m}$. A deep section

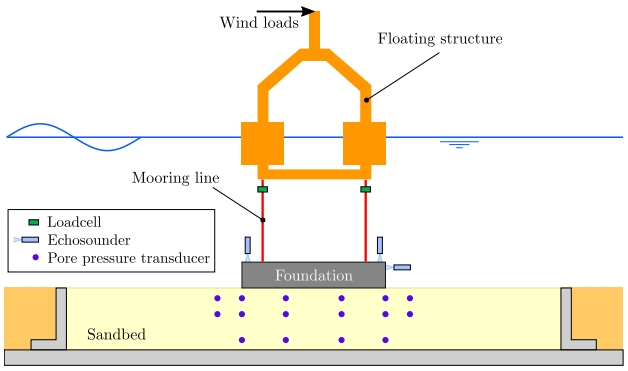

Figure 10: Schematic depiction of the large scale experimental test setup.

allows the deployment of a sand section with a length of $10\,\mathrm{m}$ and a depth of $1\,\mathrm{m}$.

During the experiments, the pore pressure, gravity anchor motion, mooring line loads, and the motion of the floating structure will be measured. To enable a realistic representation of the real–world system, wave *and* wind loads will be included in the experimental setup. While the wave loads are induced by the wave makers in the flume, the representative inclusion of the wind loads renders particularly challenging. To tackle this challenge, a hardware–in–the–loop (HIL) system will be developed.

5.2.1 Hardware–in–the–loop system

HIL systems enabling the coupling between a physical system and a numerical modelling framework are employed in various fields of engineering. For wind turbine tests in wave tanks or flumes, a HIL system is commonly employed to overcome scaling discrepancies between the wave and the wind loading.

Most striking differences between the existing systems can be observed in terms of the underlying numerical model and the actuation systems. The numerical models differ in terms of their level of non-linearity. The actuation can be based on ropes–and–pulley systems, single thrusters, or multiple fans.

For the present large scale experiments, a multi–fan system similar to [28] will be developed. The motion of the floating structure will be capture with a Qualisys motion capturing system and a linear numerical model will be employed to calculate the required thrust force, delivered by the multi-fan system. The input wind field will be based on realistic characteristics at deployment sites of the GICON® FOWT.

6 Outlook

The NuLIMAS modelling toolbox for seabed liquefaction around marine structures will have significant impact during the design of offshore structures. In future applications, the numerical model will assist in:

(i) Reducing the probability of liquefaction failures to minimize related human and economic losses

(ii) Increasing the service life of marine structures and reduce their construction costs

(iii) Reducing the risk, design uncertainty, and safety margins

(iv) Eliminating the necessity for extensive physical model testing or the use of oversimplified methods for geotechnical design

Acknowledgement

NuLIMAS receives funding through the ERA-NET Cofund MarTERA (Grant No. 728053) in the H2020 framework. Funding is also received from the German Federal Ministry for Economic Affairs and Climate Action (Grant No. 03SX524A), the Scientific and Technological Research Council of Turkey (Grant No. TEYDEB-1509/9190068), and the Polish National Centre for Research and Development (Grant MarTERA-2/NuLIMAS/3/2021).

References

[1] Aydenlou, R. M., 2020. "Chapter five - Site pathology and seismic rehabilitation methods". In *Seismic Rehabilitation Methods for Existing Buildings*, R. M. Aydenlou, ed. Butterworth-Heinemann, pp. 593–636.

[2] Christian, J. T., Taylor, P. K., Yen, J. K., and Erali, D. R., 1974. "Large diameter underwater pipe line for nuclear power plant designed against soil liquefaction". In Proceedings of the 1974 Offshore technology conference, Houston, TX, USA.

[3] Lundgren, H., L. J. H. C., and Romold, C. J., 1989. "Stability of breakwaters on porous foundation". In Proceedings of the 12th International Conference on Soil Mechanics and Foundation Engineering, Vol. 1, pp. 451–454.

[4] Muñoz-Perez, J., Khan-Mozahedy, A., Neves, M., Tejedor, B., Gomez-Pina, G., Campo, J., and Negro, V., 2015. "Sinking of concrete modules into a sandy seabed: A case study". *Coastal Engineering,* ***99***, pp. 26–37.

[5] Sumer, B. M., Hatipoglu, F., Fredsøe, J., and Sumer, S. K., 2006. "The sequence of sediment behaviour during wave-induced liquefaction". *Sedimentology,* ***53***(3), pp. 611–629.

[6] Sumer, B. M., 2014. *Liquefaction Around Marine Structures*, Vol. 39. World scientific.

[7] Biot, M. A., 1941. "General theory of three-dimensional consolidation". *Journal of applied physics,* ***12***(2), pp. 155–164.

[8] Peacock, W. H., and Seed, H. B., 1968. "Sand liquefaction under cyclic loading simple shear conditions". *Journal of the Soil Mechanics and Foundations Division,* ***94***(3), pp. 689–708.

[9] Sumer, B. M., Kirca, V. S. O., and Fredsøe, J., 2012. "Experimental validation of a mathematical model for seabed liquefaction under waves". *International Journal of Offshore and Polar Engineering,* ***22***(02).

[10] Jeng, D. S., 2003. "Wave-induced sea floor dynamics". *Appl. Mech. Rev.,* ***56***(4), pp. 407–429.

[11] Sumer, B. M., 2014. "Advances in seabed liquefaction and its implications for marine structures". *Geotech. Eng,* ***45***(4), pp. 2–14.

[12] Sumer, B. M., and Kirca, V. S. O., 2021. "Scour and liquefaction issues for anchors and other subsea structures in floating offshore wind farms: A review". *Water Science and Engineering,* ***15***, pp. 3–14.

[13] Zienkiewicz, O., Chang, C., and Bettess, P., 1980. "Drained, undrained, consolidating and dynamic behaviour assumptions in soils". *Geotechnique,* ***30***(4), pp. 385–395.

[14] Sakai, T., 1988. "Effects of inertia and gravity on seabed response to ocean waves". *Modeling Soil-Water-Structure interactions*, pp. 61–66.

[15] Raman-Nair, W., and Sabin, G., 1991. "Wave-induced failure of poroelastic seabed slopes: A boundary element study". *Proceedings of the Institution of Civil Engineers,* ***91***(4), pp. 771–794.

[16] Jeng, D.-S., Ye, J.-H., Zhang, J.-S., and Liu, P.-F., 2013. "An integrated model for the wave-induced seabed response around marine structures: Model verifications and applications". *Coastal Engineering,* ***72***, pp. 1–19.

[17] Zhao, H., Jeng, D.-S., Liao, C., and Zhu, J., 2017. "Three-dimensional modeling of wave-induced residual seabed response around a mono-pile foundation". *Coastal Engineering,* ***128***, pp. 1–21.

[18] Elsafti, H., and Oumeraci, H., 2016. "A numerical hydro-geotechnical model for marine gravity structures". *Computers and Geotechnics,* ***79***, pp. 105–129.

[19] Li, Y., Ong, M. C., and Tang, T., 2020. "A numerical toolbox for wave-induced seabed response analysis around marine structures in the OpenFOAM". *Ocean Engineering,* ***195***, p. 106678.

[20] Sumer, B. M., Fredsøe, J., Christensen, S., and Lind, M., 1999. "Sinking/floatation of pipelines and other objects in liquefied soil under waves". *Coastal Engineering,* ***38***(2), pp. 53–90.

[21] Kirca, V. S. O., 2013. "Sinking of irregular shape blocks into marine seabed under wave-induced liquefaction". *Coastal engineering,* ***75***, pp. 40–51.

[22] Kudella, M., Oumeraci, H., De Groot, M., and Meijers, P., 2006. "Large-scale experiments on pore pressure generation underneath a caisson breakwater". *Journal of waterway, port, coastal, and ocean engineering,* ***132***(4), pp. 310–324.

[23] Sumer, S. K., Sumer, B. M., Dixen, F. H., and Fredsøe, J., 2008. "Pore pressure buildup in the subsoil under a caisson breakwater". In Proceedings of the the 18th International Offshore and Polar Engineering Conference, Vancouver, Canada, OnePetro.

[24] Shanmugasundaran, R., Rusche, H., Windt, C., Kirca, V. S. O., Sumer, B. M., and Goseberg, N., 2022. "Towards the numerical modelling of residual seabed liquefaction using OpenFOAM". *Under review in the OpenFOAM Journal.*

[25] Roenby, J., 2013. *OpenFOAM library for soil mechanics*. https://github.com/roenby/soilFoam.

[26] Tang, T., Vesting, F., and Andric, J., 2012. "Implementation of solid body stress analysis in OpenFOAM". *Report for the course "CFD with OpenSource software" held at Chalmers University of Technology*.

[27] McDougal, W., Tsai, Y., Liu, P. L., and Clukey, E., 1989. "Wave-induced pore water pressure accumulation in marine soils".

[28] Urbán, A. M., and Guanche, R., 2019. "Wind turbine aerodynamics scale-modeling for floating offshore wind platform testing". *Journal of Wind Engineering and Industrial Aerodynamics,* ***186***, pp. 49–57.

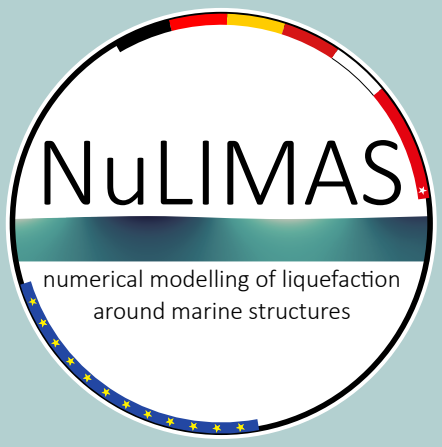

Dr. Christian Windt
Projectcoordinator
Technische Universität Braunschweig
Leichtweiß-Institute for Hydraulic Engineering and Water Resources
Division Hydromechanics, Coastal and Ocean Engineering
Beethovenstr. 51a
D-38106 Braunschweig
E-Mail: c.windt@tu-braunschweig.de
Tel.: +49531 391 3988